

Linear waveguides in photonic-crystal slabs

Steven G. Johnson, Pierre R. Villeneuve, Shanhui Fan, and J. D. Joannopoulos
*Department of Physics and the Center for Materials Science and Engineering,
 Massachusetts Institute of Technology, Cambridge, Massachusetts 02139*

(Received 25 August 1999)

Linear waveguides in photonic-crystal slabs, two-dimensionally periodic dielectric structures of finite height, are fundamentally different from waveguides in two-dimensional photonic crystals. The most important distinctions arise from the fact that photonic-crystal slab waveguides must be index-confined in the vertical direction (while a band gap confines them horizontally). We present a systematic analysis of different families of waveguides in photonic-crystal slabs, and illustrate the considerations that must be applied to achieve single-mode guided bands in these systems. In this way, the unusual features of photonic-crystal waveguides can be realized in three dimensions without the fabrication complexity required by photonic crystals with complete three-dimensional band gaps.

I. INTRODUCTION

Photonic crystals, which prohibit the propagation of light for frequencies within a band gap, have enabled exciting new ways to control light and construct integrated optical devices.¹ An important element of optical circuits is a linear waveguide to carry light to and from components, and photonic crystals also provide unique advantages for waveguides. Photonic-crystal waveguides, guided by the band gap of the bulk crystal,¹⁻⁴ can exhibit near-zero reflection and loss through sharp bends⁵ and when coupled with resonant cavities,^{6,7} due to the gap's prevention of radiation losses. Previous theoretical studies of photonic-crystal waveguides, however, have been restricted to purely two-dimensional systems and have not examined the effects of vertical confinement. In this paper, we present a systematic study of waveguide modes in a three-dimensional system, photonic-crystal slabs. Photonic-crystal slabs are two-dimensionally periodic dielectric structures of finite height that have a band gap for propagation in the plane and use index-confinement in the third dimension; they have been proposed as a more-easily fabricated alternative to true three-dimensionally periodic photonic crystals.^{2,8-19} Although their structure and properties strongly resemble those of two-dimensional crystals, slab systems require a fundamentally different, three-dimensional analysis.^{10,16,19} We will demonstrate how such analyses apply to waveguides and explain the considerations that arise for line defects in photonic-crystal slabs. We shall show that, merely to produce guided modes (as well as to be single-mode and in-gap), the parameters of the defect must be carefully chosen.

Waveguides must satisfy three criteria in order to achieve optimal performance in many integrated-optical-circuit applications; e.g., for maximum transmission through sharp bends (on the scale of the wavelength) and resonant cavities. First, of course, the waveguide must support true guided modes (as opposed to resonances, as defined later). This also implies that the waveguide structure must be periodic along the direction of propagation, in order to have a well-defined Bloch wave number k and to thereby propagate without reflections. Second, the waveguide should be single mode in

the frequency range of interest—this condition is necessary in Ref. 5 and the increased reflections in a multi-mode waveguide are a straightforward consequence of coupled-mode theory.²⁰ (Extraneous modes may have little effect if coupling to them through the bend or cavity can be made negligible, but this is not generally the case for wavelength-scale structures.) Third, the guided mode should lie within the band gap of a photonic crystal in order to prohibit radiation losses (which both decrease transmission and increase reflection²⁰); otherwise, some losses are inevitable at a bend or resonator, which breaks translational symmetry.

Conventional linear dielectric waveguides operate by index confinement (total internal reflection, in the short-wavelength limit). Such waveguides can be made to satisfy the first two criteria from above (i.e., be guiding and single-mode), and thereby have relatively high transmission through sharp bends and resonators.^{7,21,22} However, the absence of a photonic band gap means that transmission is always limited by radiation losses. In a purely two-dimensional photonic-crystal linear waveguide, a linear (one-dimensionally periodic) defect is introduced into the crystal, creating a localized band that falls within and is guided by the photonic band gap.¹⁻⁴ Light is therefore prohibited from escaping the waveguide, and all three criteria can be satisfied to achieve perfect transmission through bends and resonant cavities.⁵⁻⁷ These results have been experimentally confirmed using structures that are uniform in the third dimension for many wavelengths, and thus approximate a two-dimensional system;²³ the large aspect ratios of such geometries and their lack of vertical confinement or a true band gap in the guided modes limit their practical applications, however. There are several other possibilities for realizing photonic-crystal waveguides in three dimensions. The most ideal structure, and the only way to totally eliminate radiation losses, would be a three-dimensionally periodic structure with a complete band gap, in which the photonic crystal completely surrounds the waveguide. Such structures, though, are challenging to construct at submicron lengthscales.²⁴⁻²⁷ In this paper, we instead focus on photonic-crystal slabs. Waveguides in photonic-crystal slabs are analogous to those in two-dimensional crystals, except

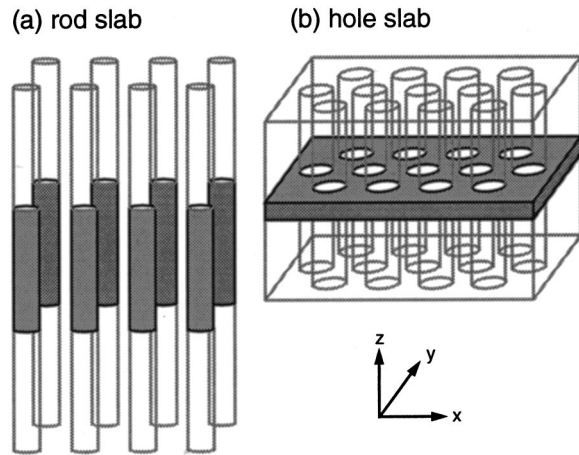


FIG. 1. Photonic-crystal slabs. (a) Square lattice of dielectric rods in air with ϵ of 12.0, lattice constant a , radius $0.2a$, and height $2.0a$, with low-index (ϵ of 2.0) rods extending infinitely above and below. (b) Triangular lattice of air holes extending through both a high-index (ϵ of 12.0) finite-height dielectric slab and low-index (ϵ of 2.0) semi-infinite dielectric regions above and below. The holes have lattice constant a and radius $0.3a$, while the high-index slab is of thickness $0.5a$.

that they use index confinement in the third dimension. Similar waveguides, which use photonic-crystal confinement in two dimensions and index confinement in the third, have been subject to experimental studies,^{28,29} as well as theoretical work subsequent to the submission of this paper.³⁰ There is also another type of photonic-crystal waveguide that we do not consider in this paper, the photonic-crystal fiber.^{31–32} This is a two-dimensionally periodic system of (in principle) infinite thickness, in which the waveguide mode propagates perpendicular to the plane of periodicity; in contrast, photonic-crystal slab waveguides are of finite thickness and run parallel to the plane of periodicity. A waveguide operating on principles similar to the fibers' was also considered in Ref. 33.

In this paper, we analyze linear-defect waveguides in two characteristic photonic-crystal slabs, a square lattice of dielectric rods in air and a triangular lattice of air holes in dielectric, illustrated in Fig. 1. Above and below the slabs are semi-infinite "extruded" substrates with the same cross sections as the slabs, but having a lower dielectric constant. (We use a substrate in order to model a more practical system than a suspended slab, and having the substrate on both sides of the slab preserves the mirror symmetry that is crucial for the existence of a gap.) The band diagrams of these two structures are given in Figs. 2 and 3, respectively; their calculation and interpretation is described in Ref. 19. Each band diagram includes a shaded region (defining the light cone) and discrete (guided) bands lying below the light cone, which are confined vertically in the vicinity of the slab by index confinement. (Thus, the slab forms a planar waveguide, but in this paper we use the term "waveguide" only to describe linear waveguides.) The presence of the light cone, with the corresponding constraint that all guided modes be index-confined in the vertical direction, gives rise to the most significant differences between photonic-crystal slabs and their two-dimensional cousins. The guided modes are either even or odd with respect to the horizontal mirror

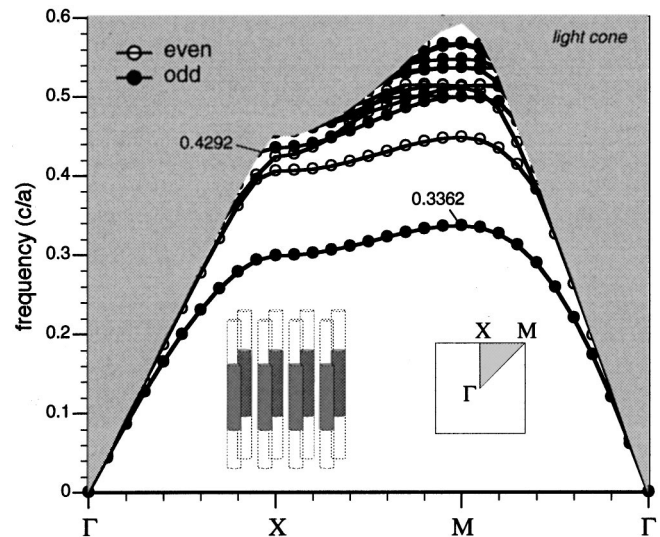


FIG. 2. Band structure for the rod slab from Fig. 1(a). Hollow and filled circles represent modes which are even and odd with respect to the horizontal ($z=0$) mirror plane bisecting the slab. There is a band gap in the odd (TM-like) modes in the frequency range $0.3362-0.4292c/a$.

symmetry plane of the slab; this is analogous to TE and TM, respectively, in two dimensions, although here the modes are not completely polarized except in the symmetry plane. The rod and hole slabs have band gaps in their odd and even modes, respectively, though these are not complete gaps due to the light cone. Nevertheless, in the gap no *guided* modes exist for the corresponding symmetry. The slab band gap has been shown to support resonant cavities in point defects,^{16,17} and we will show in this paper that it can also confine waveguide modes in linear defects. The differing thicknesses of the slabs derive from the polarizations of the modes exhibiting the band gap, and were chosen to achieve large gaps.

In order to create a linear waveguide, we break the periodicity of the slabs in one direction by creating linear defects

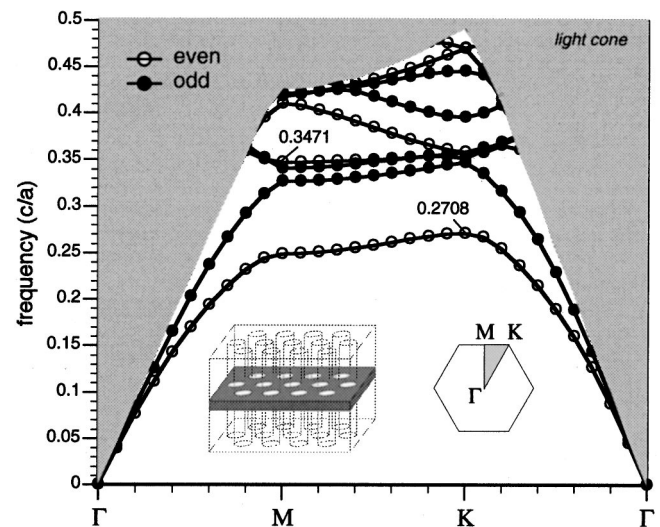


FIG. 3. Band structure for the hole slab from Fig. 1(b). Hollow and filled circles denote even and odd modes as in Fig. 2. There is a band gap in the even (TE-like) modes in the frequency range $0.2708-0.3471c/a$.

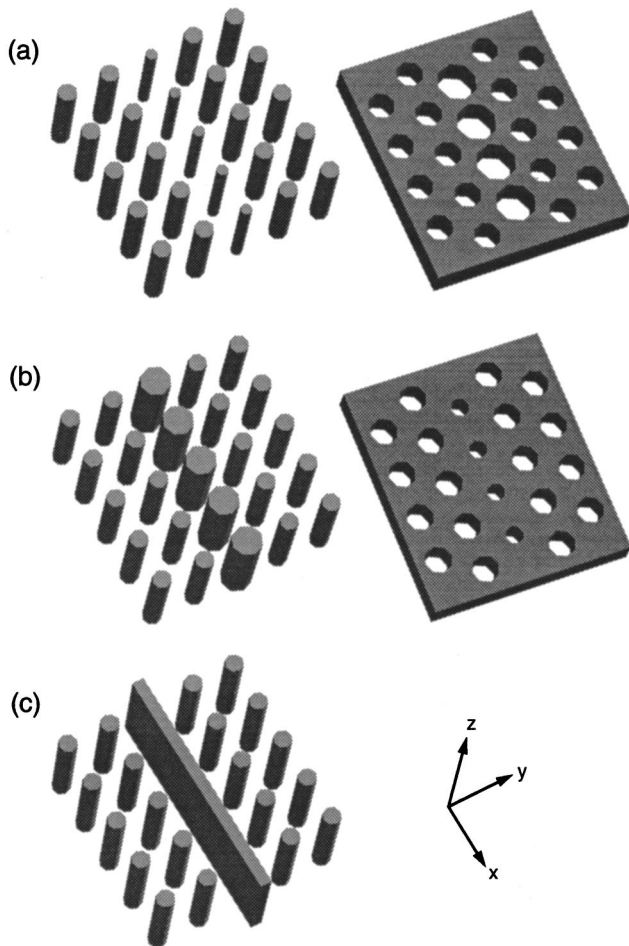


FIG. 4. Linear defects, which give rise to waveguide modes, in the rod and hole photonic-crystal slabs from Fig. 1. The low-index material is not shown, but “extrudes” above and below the structures as in Fig. 1. (a) Reduced-index waveguides, created by decreasing/increasing the radii of a line of nearest-neighbor rods/holes, respectively. (b) Increased-index waveguides, created by increasing/decreasing the radii of a line of nearest-neighbor rods/holes, respectively. (c) Dielectric-strip waveguide surrounded by the rod slab, from which a line of nearest-neighbor rods has been removed and replaced with the waveguide.

of various kinds, as shown in Fig. 4. The possible perturbations of the slab fall into two main categories: reduced-index waveguides, as in Fig. 4(a), for which the amount of high-index material is decreased; and increased-index waveguides, as in Fig. 4(b), for which the amount of high-index material is increased. We also consider a third case, shown in Fig. 4(c), in which a column of rods is removed and replaced by a conventional dielectric “strip” waveguide. In all cases, we refer to the direction along the waveguide as x , the perpendicular in-plane direction as y , and the vertical direction (out of plane) as z .

The remainder of the paper begins with a discussion of the computational methods that we employed, followed by detailed analyses of reduced-index, increased-index, and strip waveguides in photonic-crystal slabs. We then show that waveguides along nearest-neighbor directions are the most feasible. Finally, by estimating a lower bound on the fraction of the electric-field energy in the dielectric, we argue that it is not possible for photonic-crystal slabs to guide

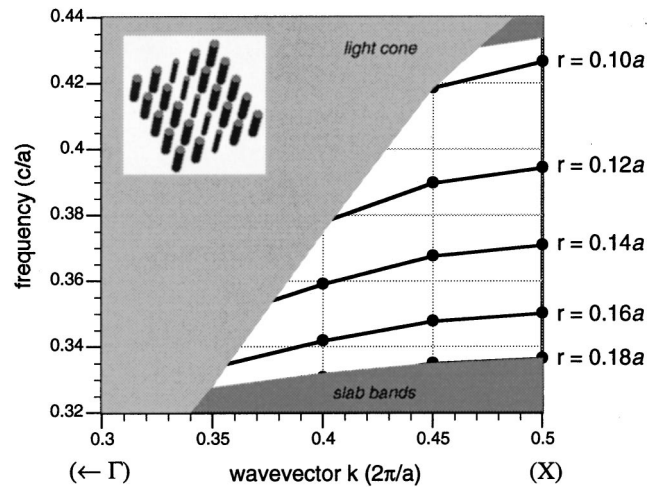


FIG. 5. Projected band structure for the reduced-index rod-slab waveguide from Fig. 4(a), showing the (odd-symmetry) guided bands for various defect rod radii (compared to the bulk radius of $0.20a$).

modes that reside primarily in air (unlike two- or three-dimensional crystals with complete gaps). (Guided modes can still reside, however, in a reduced-index region.)

II. COMPUTATIONAL METHOD

The band structures of Figs. 2 and 3 were computed as described in Ref. 19, using preconditioned conjugate-gradient minimization of the Rayleigh quotient³⁴ in a three-dimensional plane-wave basis,³⁵ with an imposed periodicity at a large interval in the vertical direction. This is a general, nonseparable, vectorial solution of the full Maxwell’s equations in a complete three dimensional basis^{36,37}—the only approximations are the discretization of the system (i.e., the planewave cutoff) and the imposition of a vertical supercell (which has a negligible effect on the localized, exponentially decaying guided modes). The light cone boundary is derived from the lowest two-dimensional band of the low-index extruded region.

Calculation of projected band structures for line defects (linear waveguides) is similar to the above, except that an additional supercell of seven or eight periods is used in the direction perpendicular to the waveguide. (Waveguide modes are sufficiently localized so that the adjacent waveguides introduced by the supercell have a negligible effect on the mode frequencies.) The bands from the unperturbed slab are projected onto the Brillouin zone of the line defect, and form the boundaries of the slab band continuum. Both the slab bands and the light cone are depicted with a uniform shading in the projected band structure, despite the varying density of states in these regions. Only modes that fall outside both the light cone and the slab bands are truly guided in the line defect, decaying exponentially away from the waveguide. When the guided bands cross into the continuum regions, they become resonances that extend infinitely away from the waveguide, albeit with low amplitude. We do not consider such resonance modes in this paper.

III. REDUCED-INDEX WAVEGUIDES

Photonic-crystal waveguides formed by removing high-index material,^{1,4,5} effectively reducing the index of the

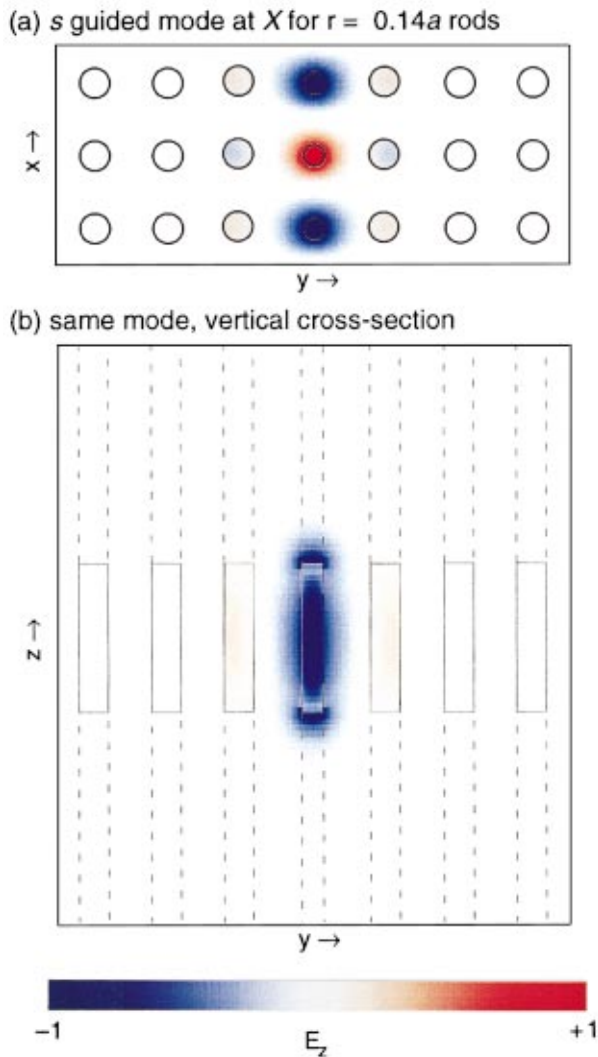


FIG. 6. (Color) Field cross sections for the rod-radius $0.14a$ guided mode at $X(0.3707c/a)$, showing the z component of the electric field. The contours of the dielectric function are shown in black. (a) Horizontal (xy) cross section in the plane bisecting the slab ($z=0$). (b) Vertical (yz) cross section in the plane perpendicular to the waveguide and bisecting a row of rods.

waveguide compared to its surroundings, are dramatic demonstrations of the photonic band gap, as they have no analogues in conventional index guiding. Such waveguides are also possible in photonic-crystal slabs, such as in Fig. 4(a) where we have reduced the radius of a line of rods or increased the radius of a line of holes. The effective index is lower in the waveguide than in the surrounding slab, so that modes can only be constrained horizontally by the band gap. On the other hand, the index is higher in the waveguide than the regions above and below the slab, so that modes can be guided vertically by index confinement. In this section, we will first consider the reduced-radius rod-slab waveguide and then the increased-radius hole-slab waveguide.

The dispersion relations for various reduced-radii rod-slab waveguides are shown in Fig. 5. There is only one guided band for each radius, so the waveguide is single mode. The line defect is periodic along its axis, and so the dispersion relation is plotted on the Γ - X reduced Brillouin zone of this lattice. The light cone and the bulk slab bands from Fig. 2

are projected onto their Γ - X wave-vector component, resulting in the continuous shaded regions of Fig. 5. This band diagram continues symmetrically beyond X , so all of the bands must have zero group velocity (slope) at X in order to be analytic functions of the wave vector. This condition of the zero slope at the Brillouin-zone edge also applies to all of the other waveguide dispersion relations that we consider in this paper. (The zero slope is not apparent in Fig. 5 because the bands were only computed at a few points.)

These discrete bands, all of odd (TM-like) symmetry, decay exponentially away from the defect because they fall in neither the light cone (vertically radiating modes) nor the continuum of odd slab bands (which propagate freely within the slab), and so cannot couple with those extended modes. This strong confinement is illustrated in Fig. 6, which depicts horizontal and vertical cross sections of the electric-field z component at X for the radius $0.14a$ line defect. We call this an s mode because the field distribution around a rod resembles an s electron state, in contrast to other waveguide modes in subsequent sections.

By the time the defect radius decreases to $0.08a$ (versus $0.20a$ in the bulk), the guided mode has entirely disappeared into the light cone. This stands in stark contrast to a two-dimensional lattice of rods, in which a line defect with the rods entirely removed still supports a guided mode.^{1,4,5} This difference is due solely to the slab's constraint of vertical index confinement—that is, the guided bands must lie outside the light cone. The two-dimensional dispersion relation of the removed-rod waveguide disappears into the upper gap edge at a wave vector of roughly $0.4(2\pi)/a$,¹ so it is not surprising that it falls into the light cone of the slab in this case. Even more generally, however, we do not expect a photonic-crystal slab waveguide to support guided modes that exist primarily in air—a large fraction of the electric field must lie within the dielectric. The basic reason for this is that the vertical confinement of the mode entails an “energy cost,” and having much of the field within the dielectric is the only way to bring the mode back down below the light cone. We quantify this argument in Sec. VII. In the case of the Fig. 5 waveguides, the fraction of the electric-field energy inside the high dielectric at X ranges from 55% for radius $0.10a$ to 68% for radius $0.18a$. (Nevertheless, the mode is still within the reduced-index region and is not index guided in the plane.)

A reduced-index waveguide in the hole slab is formed by increasing the radius of a line of nearest-neighbor holes. The resulting band diagrams for various radii are shown in Fig. 7. Here, only modes with even (TE-like) symmetry are depicted, since that is the symmetry of the bands exhibiting a gap. As with the rods, there is only a narrow range of radii that supports guided modes (all of which are single mode). Although the radius $0.40a$ band is guided, it is barely in the band gap, which begins at the maximum frequency of the lower slab bands. The projected band structure for line defects retains a wave-vector quantum number, and this means that the range of frequencies available for guided modes may be greater than the range of the band gap, as is the case here at the K' point. Since this quantum number disappears at bends and other places that break translational symmetry, however, it is important to consider only guided modes within the true band gap.

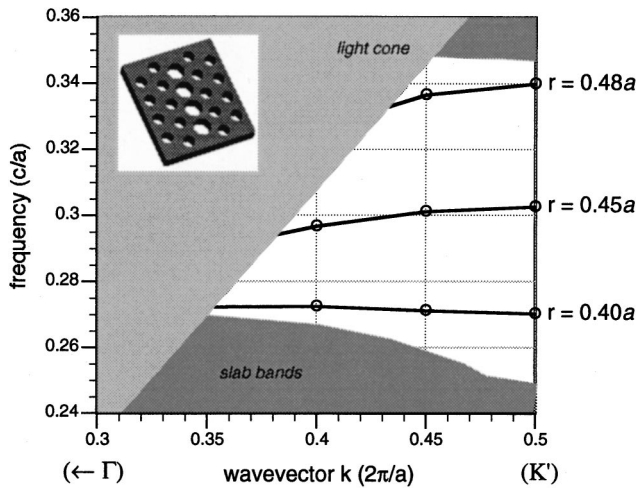


FIG. 7. Projected band structure for the reduced-index hole-slab waveguide from Fig. 4(a), showing the (even-symmetry) guided bands for various defect hole radii (compared to the bulk radius of $0.30a$).

The nearest-neighbor direction corresponds to the Γ - K direction in the slab Brillouin zone, but K is not the edge of the line-defect Brillouin zone. Figure 8 depicts how the reciprocal lattice of the slab is projected to form the reciprocal lattice of the line defect. The boundary of the projected Brillouin zone lies halfway between Γ and m' (projected from m)—this is the point K' , projected from M (which lies halfway between Γ and m). Use of the correct projection is important for the computation of the light cone and the slab bands continuum for Fig. 7.

As before, the waveguide band is s -like and strongly localized both vertically and horizontally, as shown in Fig. 9. In this case, we depict the z component of the magnetic field

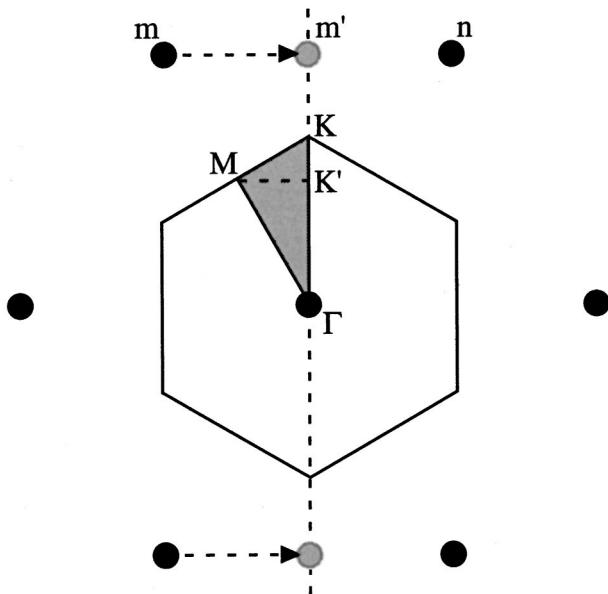


FIG. 8. Diagram of how the reciprocal lattice is projected onto Γ - K (vertical dashed line) for a nearest-neighbor line defect in the hole slab. The black dots are the reciprocal lattice points, the outlined hexagon is the first Brillouin zone, and the gray triangle within it is the reduced Brillouin zone. K' is the boundary of the first Brillouin zone in the projected lattice.

because the mode is TE-like. Since the electric field loops around the magnetic field like fields around a current, it is concentrated in the dielectric just as it was for the rods—the fraction of the electric-field energy inside the high dielectric at K' ranges from 63% for radius $0.48a$ to 86% for radius $0.40a$. The critical parameter in this case is the thickness of the narrow veins between the holes. It is only as that thickness approaches zero that the guided modes rise up far into the gap, while for small changes in defect hole radius there are no modes at all in the gap. In contrast, when the rod-slab radius is decreased, the electric field is forced directly into the air and the frequency quickly increases even for small perturbations.

There are many other ways to create reduced-index waveguides. For example, one could remove a row of rods and then shift the lattices towards one another on either side of the waveguide. This might, however, be inconvenient for applications in high-density integrated optical devices, since lattice dislocations from different components may conflict. When a row of rods is removed, one can run into additional problems due to the electric field being concentrated in the adjacent rows of remaining rods. This leads to near degeneracies between states that are even and odd with respect to the $y=0$ mirror plane, creating a multi-mode waveguide. Yet another way to create a reduced-index waveguide is to actually decrease the dielectric constant within a linear (one-dimensionally periodic) region, without necessarily changing the geometric structure.

IV. INCREASED-INDEX WAVEGUIDES

A waveguide can also be created by a line defect in which high-dielectric material is added, leading to an increased effective index. As shown in Fig. 4(b), we examine two types of increased-index waveguides: first, a rod slab with a line of increased-radius rods; and second, a hole slab with a line of decreased-radius holes. In general, increased-index defects can introduce two sorts of guided modes. First, there are modes that lie below both the light cone and the slab band continuum—these modes are conventionally index-guided horizontally as well as vertically. They do not satisfy our third waveguide criterion, however: they do not lie in the band gap, being below the lowest slab bands. Thus, we do not consider such guided bands here. The second type of guided mode, which we shall study, is a state that is pulled down into the gap from the upper slab bands. Such a mode is confined horizontally purely by the band gap and index-confined vertically, just like the reduced-index waveguides in the previous section. Because these increased-index modes derive from the upper slab bands, which have a higher density of states and often come in degenerate pairs (at symmetry points), there is a greater tendency here towards multi-mode waveguides. As we shall see, however, the single-mode criterion can be satisfied if the effective index is not increased too greatly.

Increasing the radii of a line of nearest-neighbor rods results in the band diagram of Fig. 10, showing the odd bands for rod radii of $0.25a$. This rod radius gives rise to a pair of nondegenerate guided modes, labeled p_x and p_y , but because these modes do not overlap in frequency the waveguide remains single mode. (Note that here, one can identify

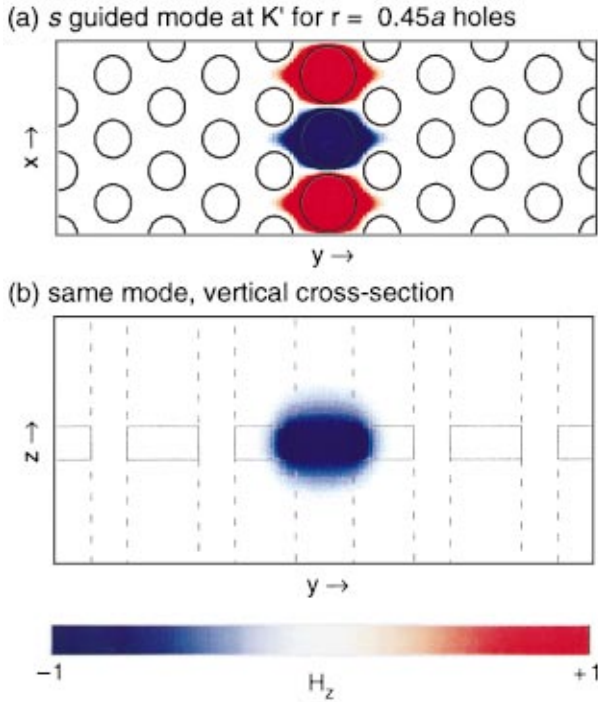


FIG. 9. (Color) Field cross sections for the hole-radius $0.45a$ guided mode at K' ($0.3026c/a$), showing the z component of the magnetic field. The contours of the dielectric function are shown in black. (a) Horizontal (xy) cross section in the plane bisecting the slab ($z=0$). (b) Vertical (yz) cross section in the plane perpendicular to the waveguide and bisecting a defect hole.

modes with the same wave vector but opposite group velocities.) Figure 11 shows cross sections of the electric field for the two states at defect radius $0.25a$. As can be seen in Fig. 11, the field around a rod is similar to a p electron state, oriented in the x and y directions for the p_x and p_y states, respectively.

When the defect rod radius is increased to $0.275a$, three additional states are pulled down into the gap, as shown in

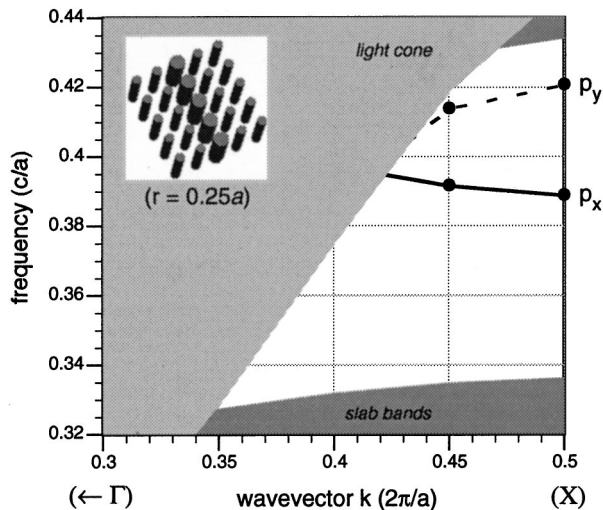


FIG. 10. Projected band structure for the increased-index rod-slab waveguide from Fig. 4(b), showing the (odd-symmetry) guided bands for defect rod radius $0.25a$ (compared to the bulk radius of $0.20a$).

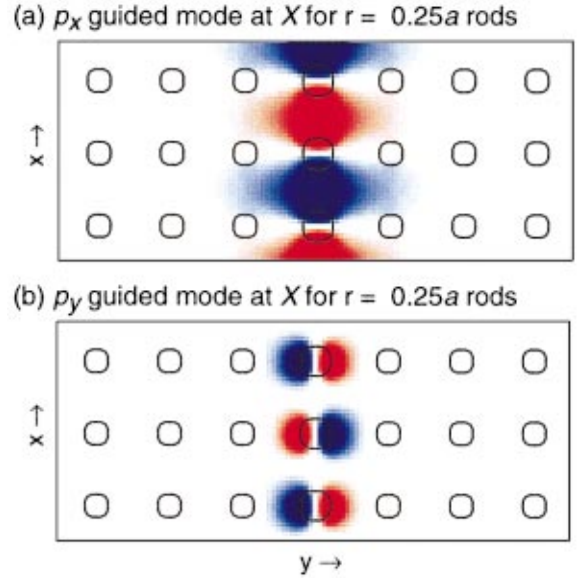


FIG. 11. (Color) Horizontal ($z=0$) E_z field cross sections for the rod-radius $0.25a$ guided modes at X . (a) p_x guided mode ($0.3887c/a$). (b) p_y guided mode ($0.4205c/a$).

Fig. 12. In this case, the p_x and p_y states cross (which is possible because they have different symmetry with respect to the $y=0$ mirror plane), meaning that they are not single mode over their whole guided range. The states labeled $p_x^{(2)}$ and $p_y^{(2)}$ have similar horizontal cross sections to p_x and p_y , but are second-order excitations in their vertical cross section (i.e., their electric fields have two vertical nodes). The state labeled $s_H^{(1)}$ is a first-order vertical excitation of the lowest TE-like band (i.e., a single vertical node in the magnetic field), which is s like in its H_z cross section. (The lowest TE-like band is of even symmetry, but adding a vertical node transforms it to odd symmetry and allows it to be guided by the gap.) The $p_x^{(2)}$, $p_y^{(2)}$, and $s_H^{(1)}$ states have no analogues in two dimensions.

Figure 13 shows the dispersion relation of even modes for the decreased-radius hole waveguides with radii of 0 , $0.15a$ and $0.25a$. The waveguides are single mode at each frequency, and there are p_x and p_y modes for each radius as for the rod slabs. In addition, the radius 0 and $0.15a$ waveguides support a higher-order d_{xy} mode. All three modes for radius $0.15a$ are depicted in Fig. 14.

In both the rod and the hole slabs, increasing the amount of dielectric brings more and more states into the gap, which makes it harder to achieve single-mode waveguides. One can ameliorate that situation by removing a row of holes and then shifting the lattices on either side of the waveguide towards one another (reducing the effective index in the waveguide). Such a waveguide was considered for the hole structure in two dimensions by Ref. 3, and similar geometries should be feasible in photonic-crystal slabs.

V. STRIP WAVEGUIDES IN PHOTONIC-CRYSTAL SLABS

In this section, we study another possible photonic-crystal slab waveguide, formed by replacing a row of rods in the

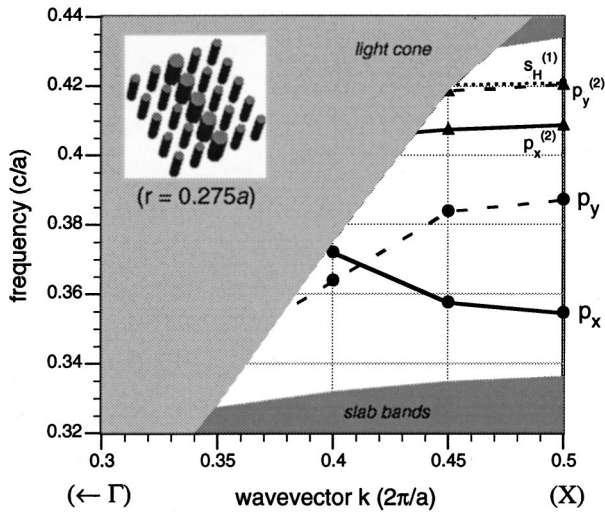


FIG. 12. Projected band structure for the increased-index rod-slab waveguide from Fig. 4(b), showing the (odd-symmetry) guided bands for defect rod radius $0.275a$.

slab of Fig. 1(a) with a conventional dielectric strip waveguide of the same thickness as the slab, as shown in Fig. 4(c). As before, there is a low-index substrate with the same cross section as the slab and waveguide both above and below this structure.

In Fig. 15 we show the odd-symmetry band diagram for such a waveguide with a width of $0.25a$. In this case, the frequency axis extends down below the slab band continuum so that both the index-guided modes (dashed lines, below the slab bands) and the gap-guided modes (solid lines) are visible. The two gap-guided modes at X are shown in Fig. 16—they differ by a 90° phase shift—and the horizontal cross sections of the index-guided modes are nearly identical to those of the gap-guided modes. The vertical cross sections of the gap- and index-guided modes differ sharply, however, as shown in Fig. 17—the index-guided mode is the fundamental mode and the gap-guided mode is a second-order excitation.

In the absence of the rod slab, both of the modes shown would lie below the light cone and be purely index-guided. Furthermore, since the strip has translational symmetry, the Brillouin zone that we apply in Fig. 15 would be artificial—the guided bands would simply fold back and forth at the zone boundaries and be degenerate at X . Because this folding is synthetic, the guided modes do not couple with the light cone even when they fold on top of it. Adding the rod slab to this system has three effects: first, the frequencies of the strip are perturbed; second, the degeneracy at X is broken by the true periodicity of the system; and third, an upper cutoff for the guided modes is introduced by the light cone (since the band folding is no longer artificial). (Also, if it were not for the band gap of the rods, the gap-guided modes would only be resonances—they would couple with the slab and leak slowly away.) Because the guided modes are strongly localized around the dielectric strip, however, the effect of the rods is small. The bands shown in Fig. 15 have an root-mean-square deviation of less than 1% from the bands of an isolated strip, and the splitting at X is also less than 1%. Because of the true periodicity of the system, the folded band structure must be analytic and the bands thus have zero group velocity at X —due to the weakness of the perturba-

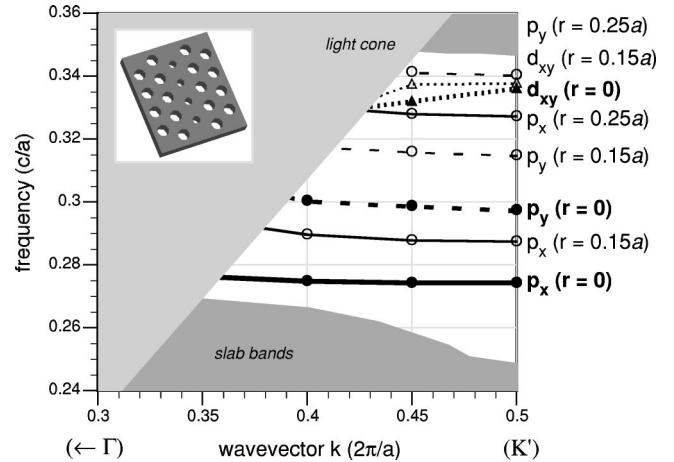


FIG. 13. Projected band structure for the increased-index hole-slab waveguide from Fig. 4(b), showing the (even-symmetry) guided bands for defect hole radii 0 , $0.15a$, and $0.25a$ (compared to the bulk radius of $0.30a$). For each radius, there are two or three guided bands: p_x (solid line), p_y (dashed line), and d_{xy} (dotted line, triangles). Guided bands for a defect hole radius of 0 , in which a row of holes is entirely removed, are shown in bold.

tion, though, the slope drops towards zero only as the wave vector comes within 1% of X . The greater the periodic perturbation, the greater the splitting and the larger the region of low group velocity, leading eventually to the highly nonlinear dispersions of the previous sections.

Despite the similarity in frequency with the modes of an isolated strip, the waveguide here has a significant advantage—it supports (single-mode) bands in the photonic band gap, which will inhibit losses in the cases of sharp bends and cavity interactions. The index-guided lower modes in this structure, on the other hand, have no advantage over a conventional waveguide. These modes might otherwise be preferred since they are the fundamental modes of the waveguide; if this is an important consideration, they can be pushed up into the band gap by reducing the waveguide width to $0.10a$ (at the expense of increased height-to-width aspect ratio).

VI. WAVEGUIDES IN OTHER DIRECTIONS

In the preceding sections, we have only considered waveguides in the nearest-neighbor directions of the slabs. Another possibility might be waveguides in the other symmetry directions (i.e., along next-nearest neighbors), as this is known to give rise to guided modes in two dimensions.⁴ Because of the presence of the light cone, however, such waveguides are not possible in the photonic-crystal slab structures of Fig. 1.

The problem is that, for the next-nearest-neighbor directions, the edge of the projected Brillouin zone comes at too small a wave vector, and the resultant folding of the light cone eliminates the band gap. For example, the next-nearest-neighbor direction in the hole slab corresponds to the M direction. When the reciprocal lattice is projected onto Γ - M , however, one of the reciprocal lattice points (n in Fig. 8) falls onto M . Therefore, the Brillouin-zone edge is at $M/2$, at which point the light-cone frequency is only $0.223c/a$. Since this upper cutoff for guided modes is lower than the gap

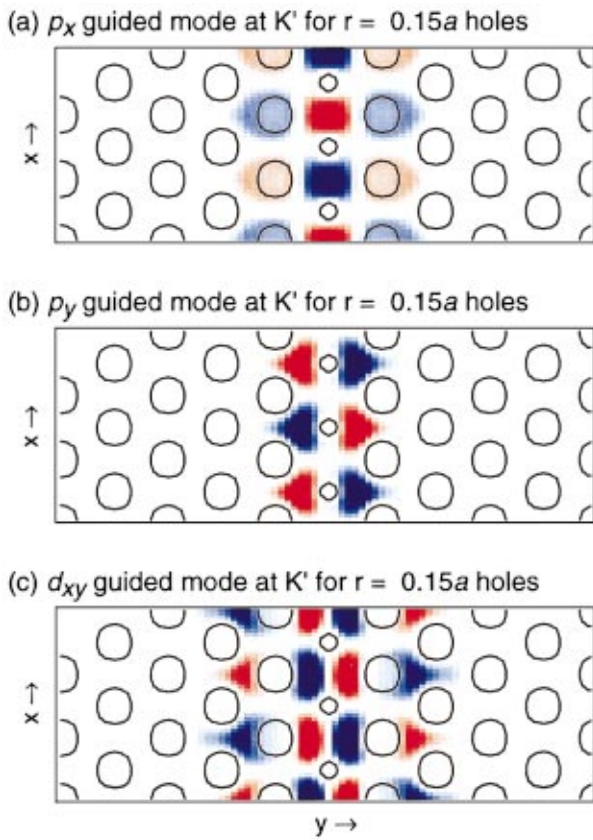


FIG. 14. (Color) Horizontal ($z=0$) H_z field cross sections for the hole-radius $0.15a$ guided modes at K' . (a) p_x guided mode ($0.2874c/a$). (b) p_y guided mode ($0.3148c/a$). (c) d_{xy} guided mode ($0.3377c/a$).

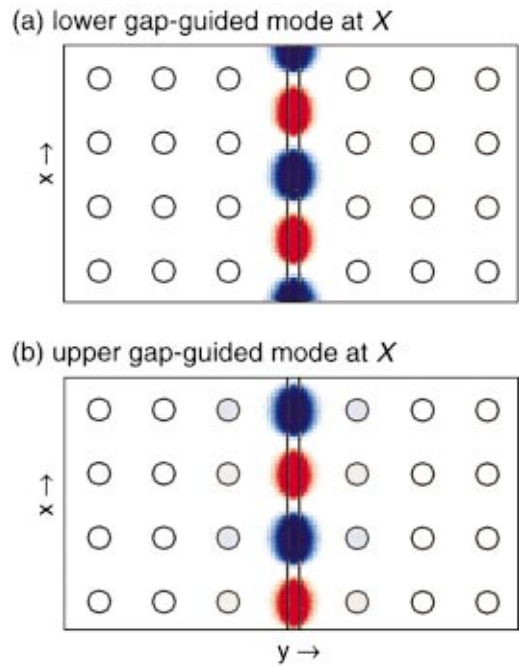


FIG. 16. (Color) Horizontal ($z=0$) E_z field cross sections for the $0.25a$ strip-waveguide gap-guided modes at X . (a) Lower gap-guided mode ($0.3626c/a$). (b) Upper gap-guided mode ($0.3629c/a$).

bottom, there is no band gap and photonic-crystal waveguides are not possible. Similarly, in the rod slab (square lattice), the Brillouin-zone boundary for the next-nearest-neighbor direction is also at $M/2$, corresponding to a light-cone frequency of $0.332c/a$ —again below the gap bottom.

If the rod slab were suspended in air (i.e., no substrate),

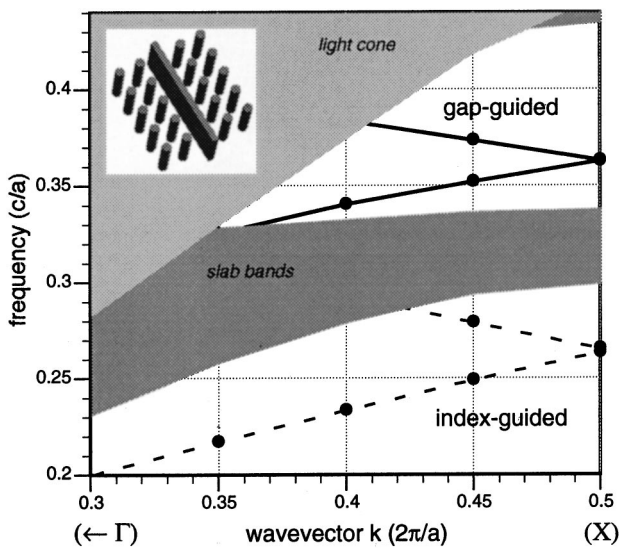


FIG. 15. Projected band structure for the strip waveguide in a rod slab, from Fig. 4(c), showing the (odd-symmetry) guided bands for waveguide width $0.25a$. There are two pairs of guided bands: gap-guided (solid lines) and index-guided (dashed lines). The gap-guided bands are split at X into a 0.07% gap, while the index-guided bands are split at X into a 0.8% gap.

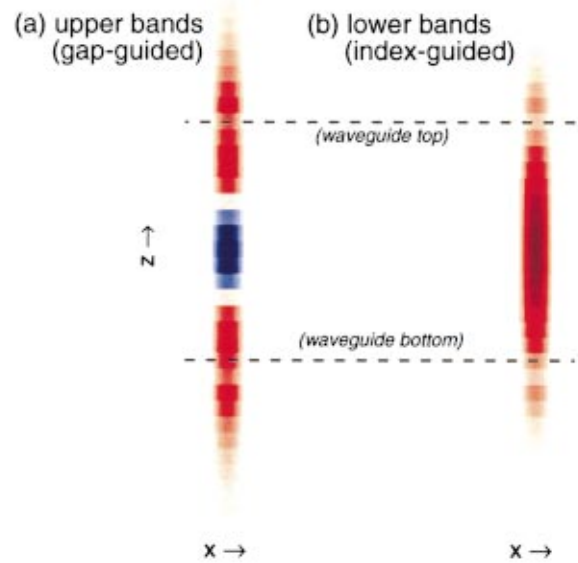


FIG. 17. (Color) Vertical ($y=0$) E_z field cross sections of a unit cell, parallel to and bisecting the waveguide, for the strip-waveguide gap-guided and index-guided modes at X . (a) Upper gap-guided mode ($0.3629c/a$). (b) Lower index-guided mode ($0.2632c/a$).

the light cone at $M/2$ would be at a frequency of $0.354c/a$, while the band-gap bottom rises to only $0.3397c/a$, leaving a slight (4%) band gap. So, in general, next-nearest-neighbor waveguides in photonic-crystal slabs are not impossible, but the available band gap is greatly reduced from the nearest-neighbor case.

VII. ESTIMATING THE FIELD ENERGY IN THE DIELECTRIC

In Sec. III, we suggested that much of the field energy must lie within the dielectric material, not in the air, in order for a waveguide mode to fall underneath the light cone and be guided. In this section, we justify that claim; moreover, we find an analytic relationship between a mode's localization and the fraction of it inside the high-index material, explaining why some waveguide modes from two-dimensional systems cannot exist in a slab. First, we derive a rigorous lower bound on the fraction of the electric field energy inside the dielectric, in terms of the spatial extent of the mode and the degree to which it is transverse. Then, we approximate the transversality and spatial confinement of the mode to compute a numerical value for this lower bound, and compare with the results of our exact calculations.

The frequency of a guided mode can be expressed as an expectation value of the Maxwell operator for the electric field, evaluated over the unit cell:

$$\omega^2 = \frac{\langle E | \nabla \times \nabla \times | E \rangle}{\langle E | \varepsilon(\vec{x}) | E \rangle}, \quad (1)$$

where we take c to be unity. Now, we suppose that the dielectric function is piecewise constant, and write the field $|E\rangle$ as a sum of fields $|E\rangle_i$, such that $|E\rangle_i$ equals $|E\rangle$ where the dielectric is ε_i and is zero elsewhere. Then, we can rewrite equation (1) as

$$\begin{aligned} \omega^2 &= \frac{\langle E | \nabla \times \nabla \times | E \rangle}{\langle E | E \rangle} \sum_i \frac{1}{\varepsilon_i} \left(\frac{\langle E | \varepsilon_i | E \rangle_i}{\langle E | \varepsilon(\vec{x}) | E \rangle} \right) \\ &= \frac{\langle E | \nabla \times \nabla \times | E \rangle}{\langle E | E \rangle} \sum_i \frac{f_i}{\varepsilon_i}. \end{aligned} \quad (2)$$

Here, f_i is the fraction of the electric field energy that is in the dielectric ε_i , and must sum to unity. In order to be guided, the frequency in Eq. (2) must be less than the light cone frequency ω_{lc} at that point in the Brillouin zone. We will write the electric field in a Fourier basis, in which case the curl operations become simply the total Fourier wave vector k squared. Because the electric field is not divergenceless, however, the curl also projects out the longitudinal field component $|E_L\rangle$, leaving only the transverse component $|E_T\rangle$. ($|E_T\rangle$ is divergenceless but not curl-free, while $|E_L\rangle$ is curl-free but not divergenceless. $|E_L\rangle$ is the static electric field of the bound charges.) In this case, the combination of Eq. (2) with the guiding constraint become:

$$\langle k^2 \rangle_{E_T} \frac{\langle E_T | E_T \rangle}{\langle E | E \rangle} \sum_i \frac{f_i}{\varepsilon_i} < \omega_{lc}^2 \leq k_B^2. \quad (3)$$

Here, k_B is the Bloch wave vector in the Brillouin zone of the line defect, and the second relation is derived from the

fact that the light cone must lie beneath the light cone of vacuum. $\langle k^2 \rangle_{E_T}$ is the mean-square wave vector of the transverse field, which is inversely related to the mode's spatial confinement. We will denote the transverse fraction of the field, $\langle E_T | E_T \rangle / \langle E | E \rangle$, by f_T . If we have a two-component system (dielectric ε and air), Eq. (3) leads to the following rigorous lower bound on the fraction of energy in the dielectric:

$$f_{\text{diel}} > \frac{1 - k_B^2 / (f_T \langle k^2 \rangle_{E_T})}{1 - 1/\varepsilon}. \quad (4)$$

The more localized the field is, the greater becomes the mean-square wave vector and the greater the minimum f_{diel} .

In order to evaluate equation (4) further, we need to estimate both f_T and a lower bound on the mean-square wavevector. We treat the wave vector by breaking it into its Cartesian components and examining each component separately (dropping the E_T subscript):

$$\langle k^2 \rangle = \langle k_x^2 \rangle + \langle k_y^2 \rangle + \langle k_z^2 \rangle. \quad (5)$$

Since the field is of the Bloch form (for a system periodic in x) and k_B is restricted to the first Brillouin zone, it can be shown that $\langle k_x^2 \rangle$ is bounded below by k_B^2 . Furthermore, we will simply drop the $\langle k_y^2 \rangle$ term, which corresponds to horizontal confinement of the waveguide mode—we consider the best case for creating a guided mode, when it is very weakly confined in the plane (e.g., near the gap edge).

$$\langle k^2 \rangle \geq k_B^2 + \langle k_z^2 \rangle. \quad (6)$$

Up to this point, we have maintained a strict lower bound on f_{diel} . Now, however, we will make two approximations. The first is based upon the observed mode profile, such as in Figs. 6 and 9. We are only interested in modes that are localized in z , so we assume that the vertical mode profile is a Gaussian with a standard deviation less than the height h of the slab, and thus

$$\langle k_z^2 \rangle \geq \frac{1}{h^2}. \quad (7)$$

Second, in the case of the rod slab, we will assume f_T to be nearly unity—that is, neglect the longitudinal component of the field. We justify this assumption by noting that the fields of the rod modes are very similar to those of the two-dimensional structure,¹⁹ in which the TM electric field is divergenceless. The only longitudinal component comes from the small regions near the rod ends where the electric field has a component normal to the dielectric surface. (For example, the rod-slab defect-radius $0.10a$ mode is 86% transverse at X .)

Finally, combining Eqs. (4), (6), and (7), we have the following approximate lower bound on the fraction of electromagnetic energy in the dielectric (for TM-like fields):

$$\text{minimum } f_{\text{diel}}^{\text{tm-like}} \approx \frac{1}{([\hbar k_B]^2 + 1)(1 - 1/\varepsilon)}. \quad (8)$$

In the case of the rod slab at the X point, this lower bound evaluates to 0.545, which is very close to the minimum of 55% that we observed for the smallest defect rod supporting

guided modes (radius $0.10a$). If we instead take f_T to be the observed value of 0.86, then the minimum f_{diel} becomes 0.457.

In contrast, let us consider the purely two-dimensional system of rods. Here, there is no light cone, so the upper-bound on the frequency is a constant ω_{max} (the top of the gap) instead of k_B . Also, there is no vertical confinement and the TM electric field is fully transverse. Thus, Eq. (4) becomes the following strict bound:

$$f_{\text{diel}}^{\text{tm}} > \frac{1 - \omega_{\text{max}}^2 / (k_B^2 + \langle k_y^2 \rangle)}{1 - 1/\epsilon}. \quad (9)$$

Therefore, for small Bloch wave vectors k_B (or for large ω_{max}) in two dimensions, it is possible to both confine in the y direction and also have a low fraction of the field in the dielectric. This corresponds precisely to what is observed in Ref. 1, in which guiding in air is demonstrated, but not near the edge of the Brillouin zone (large k_B). (Similarly, it should be possible to guide primarily in air using three-dimensional crystals with a complete band gap.)

We should emphasize that the lower bounds derived above hold for the electric-field energy, not the magnetic-field energy. Indeed, for the reduced-radius rod waveguides, we observed the fraction of the magnetic-field energy in the dielectric to drop as low as 15% (for radius $0.14a$ rods).

VIII. CONCLUDING REMARKS

Photonic-crystal slabs, with their hybrid approach of in-plane band gap combined with vertical index-confinement, promise a viable route to achieving photonic-crystal waveguide effects in real systems. We have shown how single-mode, in-gap waveguides can be achieved in a variety of ways with photonic crystal slabs. At the same time, the finite height of the slabs and restriction of index confinement have given rise to fundamentally new concerns compared to two-dimensional systems. For example, slab waveguides do not support modes guided in air or along next-nearest-neighbor directions, unlike in two dimensions. Thus, photonic-crystal slab waveguides require a full three-dimensional analysis, for which the formalism of the projected band structure provides a powerful visual and analytical tool.

ACKNOWLEDGMENTS

This work was supported in part by the Materials Research Science and Engineering Center program of the National Science Foundation under Grant No. DMR-9400334. S.G.J. would like to thank the National Defense Science and Engineering Council for financial support.

-
- ¹J. D. Joannopoulos, P. R. Villeneuve, and S. Fan, *Nature (London)* **386**, 143 (1997).
- ²R. D. Meade, A. Devenyi, J. D. Joannopoulos, O. L. Alerhand, D. A. Smith, and K. Kash, *J. Appl. Phys.* **75**, 4753 (1994).
- ³H. Benisty, *J. Appl. Phys.* **79**, 7483 (1996).
- ⁴A. Mekis, S. Fan, and J. D. Joannopoulos, *Phys. Rev. B* **58**, 4809 (1998).
- ⁵A. Mekis, J. C. Chen, I. Kurland, S. Fan, P. R. Villeneuve, and J. D. Joannopoulos, *Phys. Rev. Lett.* **77**, 3787 (1996).
- ⁶S. Fan, P. R. Villeneuve, J. D. Joannopoulos, and H. A. Haus, *Phys. Rev. Lett.* **80**, 960 (1998).
- ⁷S. G. Johnson, C. Manolatu, S. Fan, P. R. Villeneuve, J. D. Joannopoulos, and H. A. Haus, *Opt. Lett.* **23**, 1855 (1998).
- ⁸P. L. Gourley, J. R. Wendt, G. A. Vawter, T. M. Brennan, and B. E. Hammons, *Appl. Phys. Lett.* **64**, 687 (1994).
- ⁹T. Kraus, R. De La Rue, and S. Band, *Nature (London)* **383**, 699 (1996).
- ¹⁰S. Fan, P. R. Villeneuve, J. D. Joannopoulos, and E. F. Schubert, *Phys. Rev. Lett.* **78**, 3294 (1997).
- ¹¹B. D'Urso, O. Painter, J. O'Brien, T. Tombrello, A. Yariv, and A. Scherer, *J. Opt. Soc. Am. B* **15**, 1155 (1997).
- ¹²M. Kanskar, P. Paddon, V. Pacradouni, R. Morin, A. Busch, J. F. Young, S. R. Johnson, J. Mackenzie, and T. Tiedje, *Appl. Phys. Lett.* **70**, 1438 (1997).
- ¹³M. D. B. Charlton, S. W. Roberts, and G. J. Parker, *Mater. Sci. Eng. B* **49**, 155 (1997).
- ¹⁴Y. Chen, G. Faini, H. Launois, and J. Etrillard, *Superlattices Microstruct.* **22**, 109 (1997).
- ¹⁵D. Labilloy, H. Benisty, C. Weisbuch, T. F. Krauss, R. M. De La Rue, V. Bardinal, R. Houdre, U. Oesterle, D. Cassagne, and C. Jouanin, *Phys. Rev. Lett.* **79**, 4147 (1997).
- ¹⁶P. R. Villeneuve, S. Fan, S. G. Johnson, and J. D. Joannopoulos, *IEE Proc.: Optoelectron.* **145**, 384 (1998).
- ¹⁷R. Coccioli, M. Boroditsky, K. W. Kim, Y. Rahmat-Samii, and E. Yablonovitch, *IEE Proc.: Optoelectron.* **145**, 391 (1998).
- ¹⁸M. Boroditsky, R. Coccioli, and E. Yablonovitch, *Proc. SPIE* **3283**, 1 (1998).
- ¹⁹S. G. Johnson, S. Fan, P. R. Villeneuve, J. D. Joannopoulos, *Phys. Rev. B* **60**, 5751 (1999).
- ²⁰H. A. Haus, *Waves and Fields in Optoelectronics* (Prentice-Hall, Englewood Cliffs, NJ, 1984), Chap. 7.
- ²¹C. Manolatu, S. G. Johnson, S. Fan, P. R. Villeneuve, H. A. Haus, and J. D. Joannopoulos, *J. Lightwave Technol.* **17**, 1682 (1999).
- ²²J. S. Foresi, P. R. Villeneuve, J. Ferrera, E. R. Thoen, G. Steinmeyer, S. Fan, J. D. Joannopoulos, L. C. Kimerling, H. I. Smith, and E. P. Ippen, *Nature (London)* **390**, 143 (1997).
- ²³S. Y. Lin, E. Chow, V. Hietch, P. R. Villeneuve, and J. D. Joannopoulos, *Science* **282**, 274 (1998).
- ²⁴E. Yablonovitch, T. J. Gmitter, and K. M. Leung, *Phys. Rev. Lett.* **67**, 2295 (1991).
- ²⁵H. S. Sözüer and J. P. Dowling, *J. Mod. Opt.* **41**, 231 (1994).
- ²⁶K. Ho, C. Chan, C. Soukoulis, R. Biswas, and M. Sigalas, *Solid State Commun.* **89**, 413 (1994).
- ²⁷S. Fan, P. R. Villeneuve, R. Meade, and J. D. Joannopoulos, *Appl. Phys. Lett.* **65**, 1466 (1994).
- ²⁸T. Baba, N. Fukaya, and J. Yonekura, *Electron. Lett.* **35**, 654 (1999).
- ²⁹B. Temelkuran and E. Ozbay, *Appl. Phys. Lett.* **74**, 486 (1999).
- ³⁰S. Kuchinsky, D. C. Allan, N. F. Borrelli, and J.-C. Cotteverte, *Opt. Commun.* **175**, 147 (2000).
- ³¹J. C. Knight, J. Broeng, T. A. Birks, and P. St. Russell, *Science* **282**, 1476 (1998).

³²J. K. Ranka, R. S. Windeler, A. J. Stentz (unpublished).

³³O. Hanaizumi, Y. Ohtera, T. Sato, and S. Kawakami, Appl. Phys. Lett. **74**, 777 (1999).

³⁴A. Edelman and S. T. Smith, BIT **36**, 494 (1996).

³⁵R. D. Meade, A. M. Rappe, K. D. Brommer, and J. D. Joannopo-

ulos, Phys. Rev. B **48**, 8434 (1993); S. G. Johnson, *ibid.* **55**, 15 942(E) (1997).

³⁶K. M. Leung and Y. F. Liu, Phys. Rev. Lett. **65**, 2646 (1990).

³⁷Z. Zhang and S. Satpathy, Phys. Rev. Lett. **65**, 2650 (1990).